Geophys. J. R. astr. Soc. (1983) **73**, 65–82

On the vertical structure of tidal currents in a homogeneous sea

Guohong Fang *Institute of Oceanology, Chinese Academy of Sciences, Qingdao, Shandong, China*

Takashi Ichiye *Department of Oceanography, Texas A&M University, College Station, Texas 77843, USA*

Received 1982 July 1; in original form 1982 January 4

Summary. The vertical variation of tidal currents caused by friction at the sea-bed is investigated in both qualitative and quantitative ways with the Coriolis force being taken into account. The simple model with the assumption of constant eddy viscosity is employed to study the effects of friction on the vertical structure of tidal currents. The model explains these effects in vertical change of the maximum velocity, the ellipticity (the ratio of the minor to the major axis) of current ellipse, the time and the direction of the maximum velocity, and the ratio of diurnal current to semidiurnal current.

To reach a quantitative agreement with the data observed by Bowden & Fairbairn in the Irish Sea, the mixing length theory is applied to numerical calculation of the vertical distribution of tidal currents with a finite difference scheme. A fair agreement with the observations is obtained in the calculation. The results show the following features: (1) the vertical profile of amplitude of the main component for the current is almost logarithmic throughout the depth; (2) the corresponding profile for the shearing stress is almost linear with depth; (3) the maximum stress lags the maximum velocity with the delay increasing with elevation; (4) the eddy viscosity coefficient has its maximum around the mid-depth; and (5) the vertically averaged viscosity lags the velocity magnitude.

The dependence of the quadratic resistance coefficient and the coefficient κ defined by Bowden's formula $\bar{\nu} = \kappa h\bar{u}$($h$ – depth, $\bar{\nu}$ and $\bar{u}$ – depth-averaged eddy viscosity and velocity) on the roughness length is given for a steady flow in a non-rotating system. The numerical solution shows that these relations can be approximately applied to the tidal currents in shallow waters.

1 Introduction

The vertical variations of tidal currents caused by friction at the sea-bed have long been the subject by many authors. Most of the earlier works, such as Sverdrup (1926), Thorade (1931), Proudman (1953), Ichiye (1955), Bowden, Fairbairn & Hughes (1959), made use of

constant eddy viscosity coefficient and succeeded in revealing some important features of this phenomenon. In the first part the constant eddy viscosity model is used to study features of the effects of friction on the vertical structure of tidal currents. The analysis used in this part is to a certain extent similar to that of Thorade (1931, see also Defant 1961).

The simple model using constant eddy viscosity fails to produce velocity profiles quantitatively in agreement with the observed ones, especially for the layer close to the sea-bed, where the exponential profile for constant eddy viscosity does not match the observed logarithmic profile. To reach a quantitative agreement, Kagan (1964) considered ν as a function of z, which increases linearly from the bottom to a certain height, then remains unchanged up to the surface. Johns (1966, 1969a,b, 1970) took ν as a parabolic function of the depth. In these works the Coriolis force was left out. Later, Kagan (1966) employed the same function for ν about z as used in his previous paper and took the Coriolis force into account. A reasonable agreement between the theoretical solution and observed values was obtained. On the other hand, Bowden & Hamilton (1975) regarded the function ν as varying only with time. Their numerical calculations indicated that the use of variable ν very much improved the agreement with observations. It is thus worthwhile to apply Prandtl's mixing length theory directly to the calculation of the vertical distribution of tidal currents. The main reason is that Prandtl's hypothesis has been verified in various kinds of natural flows, though in most cases stationary. Further, when the mixing length hypothesis is used, the derived eddy viscosity will be variable with the depth and time. This is more reasonable according to Kagan (1965) and to Bowden & Hamilton (1975).

2 The solution with constant eddy viscosity

The equations of motion for horizontal components can be expressed as follows:

$$\begin{aligned} \frac{\partial u}{\partial t} &= fv + \frac{1}{\rho}\frac{\partial \tau_x}{\partial z} - g\frac{\partial \zeta}{\partial x}, \\ \frac{\partial v}{\partial t} &= -fu + \frac{1}{\rho}\frac{\partial \tau_y}{\partial z} - g\frac{\partial \zeta}{\partial y}, \end{aligned} \tag{2.1}$$

where the advection terms and the lateral friction are ignored, u and v are x- and y-velocity components, τ_x and τ_y the x- and y-components of the shearing stress, x, y and z the right-handed Cartesian coordinates with the z-axis vertically upwards, f the Coriolis parameter, ρ the density of the seawater, g the gravity constant and ζ the elevation of the sea surface. Variables u, v, τ_x and τ_y are functions of z and t, and the sea surface gradient components $\partial\zeta/\partial x$ and $\partial\zeta/\partial y$ are independent of z and thus the functions of t only.

The boundary conditions at the sea-bed and surface are respectively

$$\begin{aligned} &u = v = 0, \quad \text{at} \quad z = 0 \text{ (bottom)}, \\ &\tau_x = \tau_y = 0, \quad \text{at} \quad z = h \text{ (surface)}. \end{aligned} \tag{2.2}$$

Two-dimensional vectors can be conveniently expressed by complex numbers as

$$\begin{aligned} \mathbf{w} &\equiv u + iv, \\ \boldsymbol{\tau} &\equiv \tau_x + i\tau_y, \\ \mathbf{G} &\equiv -g\frac{\partial \zeta}{\partial x} - ig\frac{\partial \zeta}{\partial y}, \end{aligned} \tag{2.3}$$

where $i \equiv \sqrt{-1}$. Then (2.1) and (2.2) become respectively

$$\frac{\partial \mathbf{w}}{\partial t} + if\mathbf{w} - \frac{1}{\rho}\frac{\partial \boldsymbol{\tau}}{\partial z} = \mathbf{G}, \tag{2.4}$$

and

$$\begin{aligned} &\mathbf{w} = 0, \quad \text{at} \quad z = 0, \\ &\boldsymbol{\tau} = 0, \quad \text{at} \quad z = h. \end{aligned} \tag{2.5}$$

In order to study effects of friction on the current qualitatively, analytical solution for (2.4) is more convenient. Thus the stress is assumed to be caused by a constant eddy viscosity as

$$\boldsymbol{\tau} = \rho\nu\frac{\partial \mathbf{w}}{\partial z}, \tag{2.6}$$

where ν is a constant kinematic eddy viscosity. With (2.6) the equation (2.4) becomes

$$\frac{\partial \mathbf{w}}{\partial t} + if\mathbf{w} - \nu\frac{\partial^2 \mathbf{w}}{\partial z^2} = \mathbf{G}. \tag{2.7}$$

For the tidal currents, $\mathbf{w}$ and $\mathbf{G}$ can be expanded as Fourier series

$$\begin{aligned} \mathbf{w} &= \sum_j \{\mathbf{a}_j(z)\exp(i\sigma_j t) + \mathbf{b}_j(z)\exp(-i\sigma_j t)\}, \\ \mathbf{G} &= \sum_j [\mathbf{c}_j \exp(i\sigma_j t) + \mathbf{d}_j \exp(-i\sigma_j t)], \end{aligned} \tag{2.8}$$

where σ_j is the positive angular frequency of the jth constituent and a_j, b_j, c_j, d_j are the corresponding Fourier coefficients. Substitution of (2.8) into (2.7) and (2.5) produces

$$\begin{aligned} &i(\sigma + f)\mathbf{a} - \nu\frac{d^2\mathbf{a}}{dz^2} = \mathbf{c}, \\ &i(-\sigma + f)\mathbf{b} - \nu\frac{d^2\mathbf{b}}{dz^2} = \mathbf{d}, \end{aligned} \tag{2.9}$$

and

$$\begin{aligned} &\mathbf{a} = \mathbf{b} = 0, \quad \text{at} \quad z = 0, \\ &d\mathbf{a}/dz = d\mathbf{b}/dz = 0, \quad \text{at} \quad z = h, \end{aligned} \tag{2.10}$$

where the subscript j is omitted.

For definiteness we only consider the case of the northern hemisphere, hence f is always ≥ 0. If $f \neq \sigma$, the equations (2.9) with the boundary conditions (2.10) have the solution

$$\begin{aligned} \frac{\mathbf{a}}{\mathbf{a}_g} = 1 &- \frac{\cosh\lambda'(2h-z)\cos\lambda' z + \cosh\lambda' z\cos\lambda'(2h-z)}{\cosh 2\lambda' h + \cos 2\lambda' h} \\ &+ i\frac{\sinh\lambda'(2h-z)\sin\lambda' z + \sinh\lambda' z\sin\lambda'(2h-z)}{\cosh 2\lambda' h + \cos 2\lambda' h} \end{aligned}$$

$$\frac{\mathbf{b}}{\mathbf{b}_g} = \begin{cases} 1 - \dfrac{\cosh\lambda''(2h-z)\cos\lambda''z + \cosh\lambda''z\cos\lambda''(2h-z)}{\cosh 2\lambda''h + \cos 2\lambda''h} \\ -i\,\dfrac{\sinh\lambda''(2h-z)\sin\lambda''z + \sinh\lambda''z\sin\lambda''(2h-z)}{\cosh 2\lambda''h + \cos 2\lambda''h}, & \text{for } \sigma > f \\ 1 - \dfrac{\cosh\lambda''(2h-z)\cos\lambda''z + \cosh\lambda''z\cos\lambda''(2h-z)}{\cosh 2\lambda''h + \cos 2\lambda''h} \\ +i\,\dfrac{\sinh\lambda''(2h-z)\sin\lambda''z + \sinh\lambda''z\sin\lambda''(2h-z)}{\cosh 2\lambda''h + \cos 2\lambda''h}, & \text{for } \sigma < f \end{cases} \tag{2.11}$$

where

$$\lambda' \equiv \left(\frac{\sigma+f}{2\nu}\right)^{1/2}, \qquad \lambda'' \equiv \left(\frac{|\sigma-f|}{2\nu}\right)^{1/2} \tag{2.12}$$

and

$$\mathbf{a}_g \equiv -i\mathbf{c}/(\sigma+f), \qquad \mathbf{b}_g \equiv -i\mathbf{d}/(-\sigma+f), \tag{2.13}$$

with the subscript g representing the frictionless current.

For very deep water, i.e. $h \to \infty$, (2.11) reduces to

$$\mathbf{a}/\mathbf{a}_g = 1 - \exp(-\lambda' z)\cos\lambda' z + i\exp(-\lambda' z)\sin\lambda' z,$$

$$\mathbf{b}/\mathbf{b}_g = \begin{cases} 1 - \exp(-\lambda'' z)\cos\lambda'' z - i\exp(-\lambda'' z)\sin\lambda'' z, & \text{for } \sigma > f \\ 1 - \exp(-\lambda'' z)\cos\lambda'' z + i\exp(-\lambda'' z)\sin\lambda'' z, & \text{for } \sigma < f. \end{cases} \tag{2.14}$$

If $\sigma = f$, b_g will become infinite. However, the solution of (2.9) with conditions (2.10) for finite depth is expressed in terms of c and d as

$$\frac{\mathbf{a}}{\mathbf{c}} = \frac{-i}{\sigma+f}\left\{1 - \frac{\cosh\lambda'(2h-z)\cos\lambda' z + \cosh\lambda' z\cos\lambda'(2h-z)}{\cosh 2\lambda' h + \cos 2\lambda' h} + i\,\frac{\sinh\lambda'(2h-z)\sin\lambda' z + \sinh\lambda' z\sin\lambda'(2h-z)}{\cosh 2\lambda' h + \cos 2\lambda' h}\right\} \tag{2.15}$$

$$\frac{\mathbf{b}}{\mathbf{d}} = \frac{1}{\nu} z\left(h - \frac{z}{2}\right).$$

3 Basic characteristics of the vertical structure of tidal currents

In equation (2.8), for a single tidal constituent, the hodograph of w forms an ellipse. Variations of the resultant current w are discussed rather than the variations of the values a and b separately. The following quantities represent the characteristics of the resultant current:

M, the length of major semiaxis, or the maximum velocity;

r, the ellipticity, the ratio of minor semiaxis to major semiaxis, positive if the current rotates anticlockwise, negative if the current rotates clockwise;

θ, the direction of major semiaxis;

ζ_0, the time of maximum velocity, expressed in radian or degrees, representing the phase lag of the resultant current w.

These quantities are called ellipse parameters.

Godin (1972) has derived the relation between the ellipse parameters and the complex Fourier coefficients a and b as follows:

$$M = A + B, \tag{3.1}$$

$$r = (A - B)/(A + B), \tag{3.2}$$

$$\theta = (1/2)(\alpha + \beta), \tag{3.3}$$

$$\zeta_0 = (1/2)(\beta - \alpha), \tag{3.4}$$

where

$$A \equiv |\mathbf{a}|, \quad \alpha \equiv \arg \mathbf{a}, \quad B \equiv |\mathbf{b}|, \quad \beta \equiv \arg \mathbf{b}. \tag{3.5}$$

In order to study effects of the friction on the current ellipse under various conditions, the frictionless current is assumed given. Without loss of generality, the x-axis is taken to coincide with the major axis of the ellipse of the frictionless tidal current and the time origin is taken at the time of its maximum velocity. From this definition and (3.3–4), it follows that $\alpha_g = \beta_g = 0$. This means that both a_g and b_g are positive real numbers, or $a_g = A_g$, $b_g = B_g$.

For very deep water, the solution (2.14) is illustrated in Fig. 1. Ignoring wiggles at the upper parts of the curves, it can be seen that the functions A/A_g and B/B_g simply decrease from unity at the upper layer to zero at the bottom, and the functions α and β change from zero to $\pm 45°$. But the rates of change with elevation z are larger for the functions α and A/A_g than for the functions β and B/B_g, because $\lambda' > \lambda''$, and λ' and λ'' represent e-folding rates for the former and latter, respectively.

From (3.1–4) and with the help of Fig. 1 the following conclusions are obtained about the vertical variations of the parameters of current ellipse:

(1) The maximum velocity M reduces with an increasing depth as expected.

(2) The ellipticity r increases approaching the bottom. Thus, if the tidal current at the upper layer rotates anticlockwise, the ellipse gets broader downwards, whereas an ellipse rotating clockwise at the upper layer becomes thinner approaching the bottom and sometimes becomes a line segment or an anticlockwise ellipse. This rule has been described by

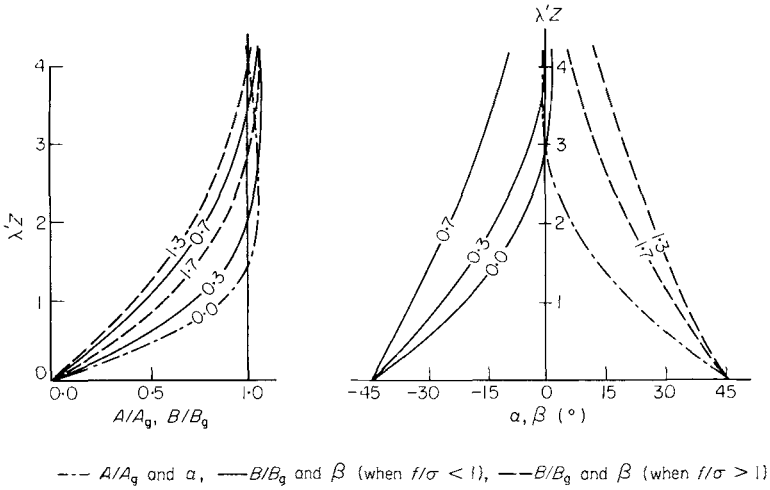

Figure 1. Vertical profiles of functions A/A_g, B/B_g, α and β. The numbers attached to curves B/B_g and β indicate the values of f/σ.

Thorade (1931). The ellipticity near the sea-bed, r_b, is expressed with the ellipticity of the frictionless current, r_g, as

$$r_b \equiv \lim_{z\to 0} r = [p'(1+r_g) - p''(1-r_g)]/[p'(1+r_g) + p''(1-r_g)], \tag{3.6}$$

where

$$p' \equiv (\sigma + f)^{1/2}, \quad p'' \equiv |\sigma - f|^{1/2}. \tag{3.7}$$

The increment of the ellipticity from $z = \infty$ to $z = 0$ is then

$$\Delta r \equiv r_b - r_g = (p' - p'')(1 - r_g^2)/[p'(1+r_g) + p''(1-r_g)], \tag{3.8}$$

which is always greater than zero unless $f = 0$ or $r_g = \pm 1$. For a certain geographic latitude, Δr cannot exceed its maximum value Δr_{max} given by

$$\Delta r_{max} = 2(p' - p'')/(\sqrt{p'} + \sqrt{p''})^2, \tag{3.9}$$

which occurs under the condition $A/B = (p''/p')^{1/2}$. For a small f/σ, the value Δr_{max} is approximately $(1/2)f/\sigma$. Therefore, for a semidiurnal tide, say, the increment of r cannot exceed roughly 0.25 at latitude 30°N, $\sqrt{2}/4$ at 45°N.

(3) In the case of $f < \sigma$, $\alpha \to 45°$ and $\beta \to -45°$ when $z \to 0$. It follows that the maximum velocity occurs earlier near the bottom than in the upper layer. An intuitive explanation of this phenomenon for $f = 0$ was first given by Proudman (1953). Equation (3.4) indicates that this time-lead caused by friction cannot exceed one eighth of the period (or 45°). The change of orientation of the ellipse axis is usually small as predicted by (3.3).

(4) When $f > \sigma$, both α and β tend to 45° as $z \to 0$. Consequently the change of the orientation angle θ becomes large and the change of the phase-lag ζ_0 of the resultant current becomes small compared to the case $f < \sigma$. From the upper layer to the bottom the direction of the ellipse axis may turn to the left up to an angle of 45°.

(5) When both diurnal and semidiurnal constituents are considered, the ratio of the maximum velocities of these two constituents determines the type of the tidal current. The analyses on the eddy viscosity in tidal current heretofore conducted have been mostly concerning the semidiurnal tide except by Ichiye (1955). Thus there are no data suitable for comparing effects of viscosity on these two constituents. The magnitude of vertical eddy viscosity may depend on the maximum current speed and time-and-space scale as well as vertical stability. However, for periodic motion with a frequency range of semidiurnal and diurnal tides there may be no serious difference in its magnitude as suggested by the results of Ichiye (1955). In the following analysis the eddy viscosity is regarded as independent of frequency.

In the absence of the Coriolis force, the ratio M_1/M_2 will decrease with the depth and tend to $(\sqrt{2}/2)(M_{1g}/M_{2g})$ as $z \to 0$, where the subscripts 1 and 2 indicate the diurnal and semidiurnal constituents, respectively. For the general case, its variation with depth is dependent on the Coriolis parameter and the ellipticities of these two constituents. The limit of M_1/M_2, for $z \to 0$, is

$$\lim_{z\to 0} \frac{M_1}{M_2} = \lim_{z\to 0} \frac{A_1 + B_1}{A_2 + B_2} = C\frac{M_{1g}}{M_{2g}}, \tag{3.10}$$

with

$$C = \frac{p_1'(1+r_{1g}) + p_1''(1-r_{1g})}{p_2'(1+r_{2g}) + p_2''(1-r_{2g})}. \tag{3.11}$$

Table 1. The factor C for various latitudes in the case of $r_{1g} = r_{2g} = 0$.

$\phi(^\circ)$	0	10	20	30	40	50	60	70	80	90
C	0.71	0.70	0.67	0.52	0.77	0.91	1.02	1.14	1.25	1.37

The values of C are independent of ν and thus are listed in Table 1 for various latitudes ϕ in the case of $r_{1g} = r_{2g} = 0$, where the approximations $\sigma_1 = 1/2\ \sigma_2$ and $f = \sigma_2 \sin\phi$ have been used.

It is then expected that the ratio M_1/M_2 usually decreases with increasing depth at low and middle latitudes and increases with depth at high latitudes. But the except is possible, because the factor C is also dependent on r_{1g} and r_{2g}. It is sometimes observed at low and middle latitudes that the type of tidal current is diurnal near the surface but becomes of mixed type near the bottom, or of mixed type near the surface but becomes semidiurnal near the bottom. Reverse situations may occur at high latitudes, though there is no definite observed evidence.

For the finite depth water, the solution a/a_g is shown in Fig. 2. This figure indicates that the depth does not change the feature that the magnitude of a reduces and the argument of a increases towards the sea-bed. However, the magnitude of the changes from surface to bottom is smaller in the shallow water than in the deep water. This rule also hold for the function b/b_g. It follows that an effect of the finite depth is only to reduce the differences between the upper and lower layers.

For the case of $f = \sigma$, the solution (2.15) indicates that the argument of b is independent of z, therefore both the direction of the ellipse axis θ and the phase-lead of the resultant current $-\zeta_0$ are equal to $(1/2)\alpha$. This means that the direction of the ellipse axis at the layer very near the bottom deviates to the left of the one at the surface by up to 22.5°, and the maximum velocity at that layer occurs earlier than at the surface by up to one-sixteenth of the period.

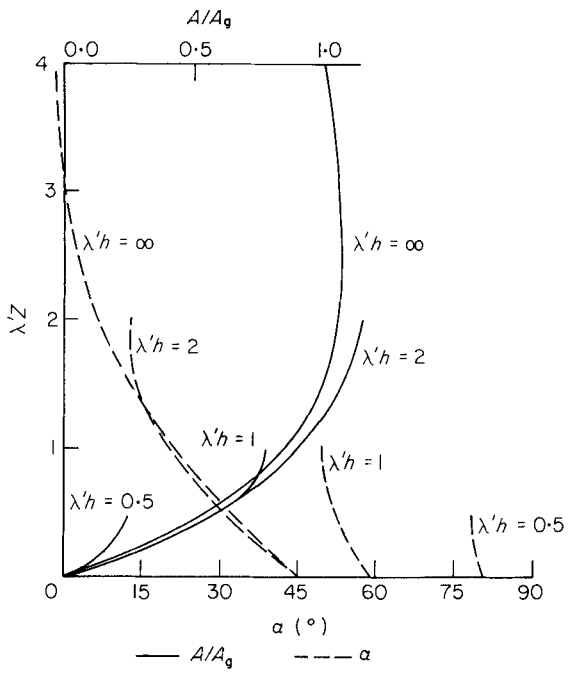

Figure 2. Functions A/A_g and α for the sea of various depths.

4 Application of the mixing length theory to calculation of the tidal current

The constant eddy viscosity models may be too simplified to produce observed vertical structures of tidal currents. Thus Prandtl's hypothesis of the shearing stress is extended to a two-dimensional unsteady flow as

$$\tau = \rho l^2 \left|\frac{\partial \mathbf{w}}{\partial z}\right| \frac{\partial \mathbf{w}}{\partial z}, \tag{4.1}$$

where l represents a mixing length. If l is taken as a real function of z, expression (4.1) implies that the stress is parallel to the velocity gradient and the stress changes periodically in phase with the velocity gradient. A more complicated and probably more accurate relation than (4.1) is not warranted considering the quality of data available so far.

For the layer in the vicinity of the boundary, Prandtl assumed the mixing length l to vary directly with the distance as

$$l = k_0(z + z_0), \tag{4.2}$$

where k_0 is the Karman constant approximately equal to 0.4, and z_0 is the roughness length. From the measured velocity profile in pipes with a circular cross-section, Nikuradse (1933, see Schlichting 1968, p. 568) found that relation (4.2) should be revised so that the ratio of the mixing length to the distance from the boundary decreases with increasing distance. Montgomery (1943) proposed a hypothesis by taking the shape of the cross-section into account. Applying this hypothesis to a circular cylinder, he obtained a formula for a mixing length in good agreement with Nikuradse's empirical formula. Reid (1957) adopted Montgomery's hypothesis for a steady flow in a non-rotating wide channel. He assumed that the water surface was also the fixed boundary and took l as

$$l = (k_0/h)(z + z_0)(h - z + z_1), \tag{4.3}$$

where z_1 is the roughness parameter at the surface and very small compared with the water depth. Since the free surface is unlikely to impose restriction on the turbulence to the same extent as the sea-bed does, and there is no solid information on z_1 in relation to other factors like wind or waves, z_1 is neglected in the present investigation. Instead a parameter μ is introduced as

$$l = k_0(z + z_0)(1 - z/\mu h) \quad (\mu > 1). \tag{4.4}$$

This function has its maximum at $z = (1/2)\mu h$ ($z_0 \ll \mu h$), zero at $z = \mu h$, which is on or above the surface. When $\mu = 1$, (4.4) reduces to (4.3) with z_1 negligible, when μ tends to infinity, it becomes (4.2).

Both (4.3) and (4.4) tend to (4.2) in the vicinity of the bottom, where the value of l becomes more crucial for the vertical velocity distribution than at the upper layer.

Equations (2.4), (4.1) with boundary conditions (2.5) form a complete set of differential equations for determining the vertical structure of the tidal currents.

5 Quadratic resistance and eddy viscosity coefficients for a steady flow

A steady flow caused by a uniformly sloped sea-level is considered without the Coriolis effect in order to determine relationships among the mixing length given by (4.4), the vertical profiles, the eddy viscosity and the bottom friction.

In this case, the first two terms of (2.4) vanish and the shearing stress should be a linear function of z:

$$\tau = \tau_b(1 - z/h), \tag{5.1}$$

with τ_b representing the stress at the sea-bed.

From (4.1), (4.4) and (5.1) we have

$$\frac{du}{dz} = \frac{u_*}{k_0} \frac{\sqrt{1-z/h}}{(z+z_0)(1-z/\mu h)}, \tag{5.2}$$

where $u_* \equiv (\tau_b/\rho)^{1/2}$ is the friction velocity. The integral of (5.2) is

$$u = \frac{u_*}{k_0} \left\{ \ln \frac{4(1-\sqrt{1-z/h})}{(z_0/h)(1+\sqrt{1-z/h})} - 2\sqrt{\mu-1} \left(\arctan \frac{1}{\sqrt{\mu-1}} - \arctan \frac{\sqrt{1-z/h}}{\sqrt{\mu-1}} \right) \right\}, \tag{5.3}$$

where the condition $z_0/h \ll 1$ has been used. When $\mu \to \infty$, i.e. (4.2) is valid, (5.3) reduces to

$$u = \frac{u_*}{k_0} \left\{ \ln \frac{4(1-\sqrt{1-z/h})}{(z_0/h)(1+\sqrt{1-z/h})} - 2(1-\sqrt{1-z/h}) \right\}. \tag{5.4}$$

When $\mu = 1$, i.e. (4.3) is applicable, (5.3) reduces to

$$u = \frac{u_*}{k_0} \ln \frac{4(1-\sqrt{1-z/h})}{(z_0/h)(1+\sqrt{1-z/h})}. \tag{5.5}$$

For the general case, the second term of (5.3) is usually smaller by one order of magnitude than the first term. In the layer near the bottom, $z/h \ll 1$, and (5.3) reduces to

$$u = \frac{u_*}{k_0} \ln \frac{z}{z_0}, \tag{5.6}$$

which is the well-known logarithmic profile and is independent of μ.

The depth-averaged velocity of (5.3) is

$$\bar{u} \equiv \frac{1}{h} \int_0^h u\,dz = \frac{u_*}{k_0} \left[\ln \frac{4h}{z_0} - 2\mu + 2(\mu-1)^{3/2} \arctan (\mu-1)^{-1/2} \right]. \tag{5.7}$$

When $\mu \to \infty$, (5.7) becomes

$$\bar{u} = \frac{u_*}{k_0} \left(\ln \frac{4h}{z_0} - \frac{8}{3} \right). \tag{5.8}$$

When $\mu = 1$, (5.7) becomes

$$\bar{u} = \frac{u_*}{k_0} \left(\ln \frac{4h}{z_0} - 2 \right), \tag{5.9}$$

which has been obtained by Reid (1957).

As pointed out by Reid (1957), the resistance coefficient R is defined by

$$\tau_b = R\rho |\bar{u}| \bar{u}, \tag{5.10}$$

and thus this coefficient can be expressed in terms of μ and z_0 from (5.7) as

$$R = k_0^2 [\ln(4h/z_0) - 2\mu + 2(\mu-1)^{3/2} \arctan (\mu-1)^{-1/2}]^{-2}. \tag{5.11}$$

The numerical relation is shown in Table 2. Reid (1957) determined the relation between R and z_0 from (5.9) which corresponds to the first column of Table 2.

The coefficient of eddy viscosity, defined by $\nu = \tau/\rho(\partial u/\partial z)$, is then

$$\nu = k_0 u_* (z+z_0)(1-z/\mu h)\sqrt{1-z/h}. \tag{5.12}$$

It is zero at the surface, has very small value $k_0 u_* z_0$ at the bottom, and has the maximum

Table 2. The quadratic resistance coefficient R defined by (5.10) and Bowden's turbulence coefficient κ defined by (5.14) as the functions of h/z_0 and μ for steady flows in a non-rotating system.

$\lg h/z_0$	$\mu = 1.0$	1.2	1.5	2.0	4.0	∞	$\mu = 1.0$	1.2	1.5	2.0	4.0	∞
	$R \times 10^3$						$\kappa \times 10^3$					
2.0	10.04	11.10	11.90	12.61	13.58	14.47	4.58	5.89	7.20	8.56	10.65	12.83
2.2	8.07	8.83	9.39	9.89	10.56	11.17	4.11	5.26	6.40	7.58	9.40	11.27
2.4	6.63	7.19	7.60	7.96	8.44	8.88	3.72	4.74	5.76	6.80	8.40	10.05
2.6	5.54	5.97	6.28	6.55	6.90	7.22	3.40	4.32	5.23	6.17	7.59	9.06
2.8	4.70	5.03	5.28	5.48	5.75	5.99	3.13	3.96	4.80	5.64	6.93	8.26
3.0	4.04	4.30	4.49	4.65	4.86	5.05	2.91	3.66	4.42	5.20	6.37	7.58
3.2	3.51	3.72	387	4.00	4.17	4.32	2.71	3.41	4.11	4.82	5.90	7.01
3.4	3.07	3.25	3.37	3.47	3.61	3.73	2.53	3.19	3.83	4.49	5.49	6.51
3.6	2.72	2.86	2.96	3.05	3.16	3.26	2.38	3.00	3.59	4.21	5.14	6.09
3.8	2.42	2.54	2.62	2.69	2.79	2.87	2.25	2.82	3.38	3.95	4.83	5.71
4.0	2.16	2.27	2.34	2.40	2.48	2.54	2.13	2.66	3.19	3.73	4.55	5.38
4.2	1.95	2.04	2.10	2.15	2.22	2.27	2.02	2.52	3.03	3.53	4.31	5.08
4.4	1.77	1.84	1.89	1.94	1.99	2.04	1.92	2.40	2.87	3.36	4.08	4.82
4.6	1.61	1.67	1.72	1.75	1.80	1.85	1.83	2.28	2.74	3.19	3.88	4.59
4.8	1.47	1.52	1.56	1.60	1.64	1.68	1.75	2.18	2.61	3.05	3.70	4.37
5.0	1.35	1.40	1.43	1.46	1.50	1.53	1.68	2.09	2.50	2.91	3.54	4.17
5.2	1.24	1.28	1.31	1.34	1.37	1.40	1.61	2.00	2.39	2.79	3.38	3.99
5.4	1.15	1.18	1.21	1.23	1.26	1.29	1.55	1.92	2.30	2.67	3.25	3.83
5.6	1.06	1.10	1.12	1.14	1.16	1.19	1.49	1.85	2.21	2.57	3.11	3.68
5.8	0.99	1.02	1.04	1.06	1.08	1.10	1.44	1.78	2.13	2.48	3.00	3.54
6.0	0.92	0.95	0.96	0.98	1.00	1.02	1.39	1.72	2.05	2.39	2.89	3.41

value at a mid-depth. The vertically averaged value of ν is

$$\bar{\nu} \equiv \frac{1}{h}\int_0^h \nu dz = \frac{4}{15}\left(1 - \frac{4}{7}\frac{1}{\mu}\right) k_0 u_* h, \tag{5.13}$$

where the relation $z_0 \ll h$ has been used. Bowden (1962, see also Bowden & Hamilton 1975) has suggested on the basis of dimensional analysis that the maximum eddy viscosity can be expressed as proportional to the product of the water depth and the velocity. He found that the proportional factor in the region near Anglesey was 2.5×10^{-3}. Relation between the mean eddy viscosity and the mean velocity seems to be more practical and is expressed by

$$\bar{\nu} = \kappa h \bar{u}, \tag{5.14}$$

where κ is a dimensionless coefficient and may be called the Bowden turbulence coefficient. For a steady flow in non-rotating system, κ can be obtained from (5.10) and (5.13) as follows:

$$\kappa = \frac{4}{15}\left(1 - \frac{4}{7}\frac{1}{\mu}\right) k_0 R^{1/2}, \tag{5.15}$$

which, like R itself, also depends on h/z_0 and μ and is listed in Table 2.

For the layer near the bottom, (5.12) tends to

$$\nu = k_0 u_*(z + z_0) = k_0 R^{1/2} \bar{u}(z + z_0), \qquad \text{for } z \ll h, \tag{5.16}$$

which is the same form as for the logarithmic profile, as it should be.

6 Difference scheme for the calculation of the vertical distribution of tidal current

The vertical distribution of the current is highly sensitive to the roughness length z_0. Therefore the grid spacing along the z-direction should be comparable to z_0 in the neighbourhood of the sea-bed. To avoid using too many grid points we introduce the transform

$$s \equiv \ln(1 + z/z_0), \tag{6.1}$$

where $s = 0$ at $z = 0$ and $s = \ln(1 + h/z_0) \equiv s_h$ at $z = h$. Substitution of s for z changes equations (2.4) and (4.1) into

$$\begin{aligned} &\frac{\partial \mathbf{w}}{\partial t} + if\mathbf{w} - \frac{\partial \tau'}{\partial s}\exp[-(s + s_0)] = \mathbf{G}, \\ &\tau' = l^2 \left|\frac{\partial \mathbf{w}}{\partial s}\right| \frac{\partial \mathbf{w}}{\partial s}\exp[-2(s + s_0)], \end{aligned} \tag{6.2}$$

where s_0 and $\boldsymbol{\tau}'$ represent $\ln z_0$ and $\boldsymbol{\tau}/\rho$ respectively.

An implicit finite difference scheme is employed to avoid possible computational instability. The mesh used in the present investigation is shown in Fig. 3. This arrangement makes the calculation and the boundary condition (2.5) simpler. For all n (2.5) becomes

$$\begin{aligned} &\mathbf{w}_1^n = 0, \\ &\boldsymbol{\tau}_m'^n = 0. \end{aligned} \tag{6.3}$$

The difference equations are

$$\begin{aligned} &\frac{\mathbf{w}_m^n - \mathbf{w}_m^{n-1}}{\Delta t} - \frac{\boldsymbol{\tau}_m'^n - \boldsymbol{\tau}_{m-1}'^n}{\Delta s}\exp[-(s_{m_1} + s_0)] + \frac{i}{2} f(w_m^n + w_m^{n+1}) = G^n, \\ &\tau_m'^n = (l_m)^2 \left|\frac{\mathbf{w}_{m+1}^{n-1} - \mathbf{w}_m^{n-1}}{\Delta s}\right| \frac{\mathbf{w}_{m+1}^n - \mathbf{w}_m^n}{\Delta s}\exp[-2(s_{m_2} - s_0)]. \end{aligned} \tag{6.4}$$

where s_{m_1} and s_{m_2} represent the values of s at the points w_m and τ_m', respectively.

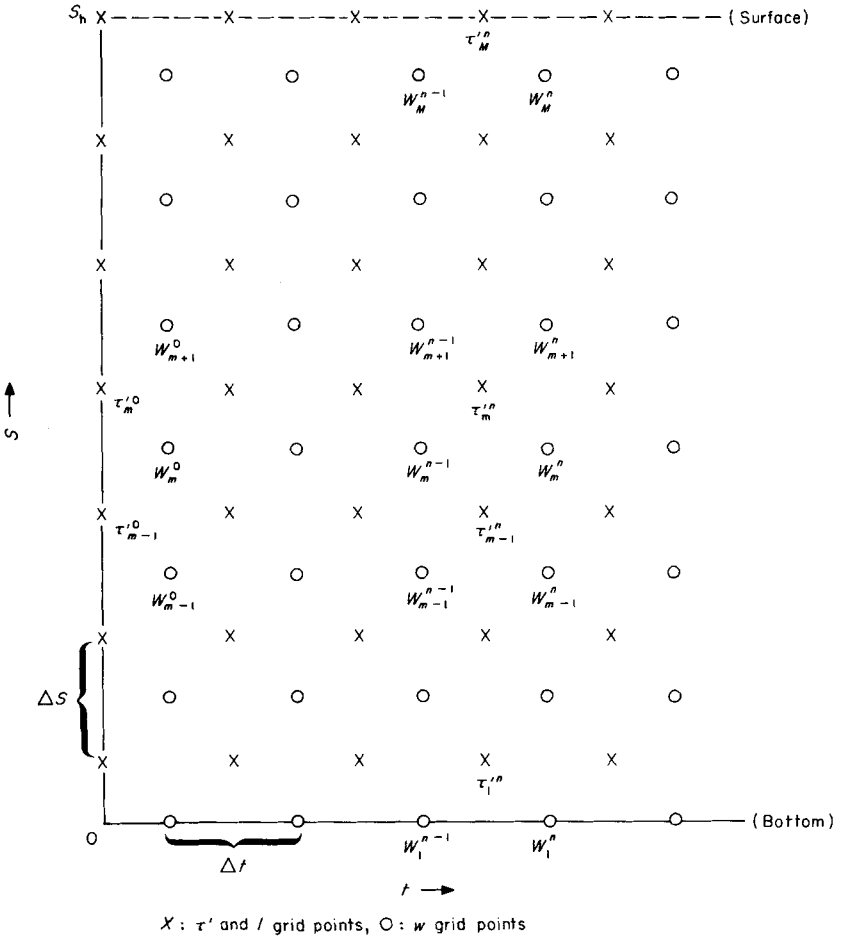

Figure 3. Computational mesh.

After rearrangement, the difference equations are written

$$\tau'^{n}_{m-1} + \left[\Delta s\left(\frac{1}{\Delta t} + \frac{i}{2}f\right)\exp(s_{m_1} + s_0)\right]\mathbf{w}^{n}_{m} - \tau'^{n}_{m}$$

$$= \left[\Delta s\left(\frac{1}{\Delta t} - \frac{i}{2}f\right)\exp(s_{m_1} + s_0)\right]\mathbf{w}^{n-1}_{m} + [\Delta s\exp(s_{m_1} + s_0)]\,\mathbf{G}^{n},$$

$$\mathbf{w}^{n}_{m} + \left[\frac{\Delta s\exp(s_{m_2} + s_0)}{l_m}\right]^2 \frac{1}{|\mathbf{w}^{n-1}_{m+1} - \mathbf{w}^{n-1}_{m}|}\,\tau'^{n}_{m} - \mathbf{w}^{n}_{m+1} = 0. \tag{6.5}$$

For a specific n, (6.4) and (6.5) constitute a set of linear algebraic equations with a tridiagonal matrix, though its elements are complex numbers. For simplicity the initial condition is taken as

$$\tau'^{0}_{m} = \mathbf{w}^{0}_{m} = 0, \qquad \text{for } m = 1, 2, \ldots, M. \tag{6.6}$$

When a single tidal constituent is considered, it is recommended to use time spacing

$$\Delta t = T/(12N), \tag{6.7}$$

where N is an integer and T the period of the constituent. This means that the period is divided into $12N$ steps. By comparing w_m^n with w_m^{n-12N} stable periodicity can be verified. If the differences for all $m = 1, \ldots, M$ are sufficiently small, computation is judged to produce the stable periodic state. If several constituents are considered, Δt may be taken as the common period of the constituents divided by an appropriate integer.

In solving (6.5), the quantity z_0 and function G must be given. The roughness length can be determined empirically by the sediment characteristic and the configuration of the sea-bed (see, for example, Heathershaw 1979). However, the sea surface slope is difficult to measure. There are a few alternatives to apply the preceding difference method to an actual situation.

(1) For the deep ocean, when currents are measured at several depths including the upper layers, which are located far from the bottom boundary layer, then the current averaged over such layers can be assumed to represent w_g, which are free from the bottom friction. The function G is thus obtained from (2.4) by omitting the friction term and substituting w_g for w. The thickness of the bottom boundary layer depends on the current magnitude and roughness parameter, but in general is considered as several metres in the deep ocean (Wimbush & Munk 1980).

(2) For the shallow water, where the bottom friction can influence the current at the upper layer, G may be estimated from the vertically averaged observed velocity. Averaging (2.4) from $z = 0$ to h gives

$$\mathcal{G} = \frac{\partial \bar{w}}{\partial t} + if\bar{w} + \frac{\tau_b'}{h}. \tag{6.8}$$

The stress at the bottom can be given approximately by

$$\tau_b' \approx R\,|\bar{w}|\,\bar{w}. \tag{6.9}$$

If R is assumed to be the same as that for a non-rotating channel, then it can be obtained from Table 2. Because of the inadequacy of (6.9) and the inaccuracy of the coefficient R, the function G thus obtained is only an estimate. When it is used for numerical calculation, the calculated depth-averaged velocity will differ from the observed velocity $\bar{w}$. Therefore, adjustment for G is usually necessary. Further details will be shown in an example in the next section, where R is given and z_0 is derived from R and $\bar{w}$. In the literature on ocean tides the parameter R seems to be better estimated than the parameter z_0.

7 A comparison of the calculated result with the observed current

Careful measurements were carried out in the Irish Sea by Bowden & Fairbairn (1952, hereafter referred as BF). The data obtained at the East station have relatively smaller variances compared to those at the West station and consequently are used for the basis of numerical calculation. To minimize observational errors four groups of the harmonics are averaged and listed in Table 3 along with the depth-averaged harmonics, where U and ξ are amplitude and phase-lag of semidiurnal constituent of u, V and η are those of v.

In the calculation the values of μ, h, σ and f are taken as 1.2, 15.4 m, $1.405 \times 10^{-4}\ s^{-1}$ and $1.170 \times 10^{-4}\ s^{-1}$, respectively. The quadratic resistance coefficient R is estimated from the measurements by BF as

$$R = \frac{3\pi}{8} \times \frac{2.01 + 2.04 + 1.42}{3} \times 10^{-3} = 2.15 \times 10^{-3}. \tag{7.1}$$

The factor $3\pi/8$ is added since the three numerical values are obtained by assuming $\tau_b' = F_b \sin \sigma t$, say, for a constituent of frequency σ, whereas the bottom stress given by (6.9) should be $\tau_b' = (3\pi/8) F_b \sin \sigma t\,|\sin \sigma t|$.

Table 3. Comparison of calculated harmonic constants to observed values.

Fraction of depth	Observed harmonics U (cm s^{-1})	ξ (°)	V (cm s^{-1})	η (°)	Calculated harmonics U (cm s^{-1})	ξ (°)	V (cm s^{-1})	η (°)
0.25	62.8	2.5	23.3	12.1	62.9	1.4	21.5	12.5
0.50	59.3	0.1	21.7	12.0	59.6	0.5	20.9	12.4
0.75	53.5	−0.9	16.8	12.6	54.2	−0.4	19.6	12.0
0.95	44.7	−1.2	13.6	13.3	43.0	−1.7	16.0	11.6
Depth-averaged	57.4	0.6	20.2	12.3	57.4	0.5	20.2	12.3

The first approximation of G is given by equations (6.8) and (6.9) with

$$\bar{w} = 57.4 \cos(\sigma t - 0.^{\circ}6) + i\, 20.2 \cos(\sigma t - 12.^{\circ}3), \tag{7.2}$$

where the harmonic constants are taken from Table 3. For a steady flow in a non-rotating channel with a depth 15.4 m, the roughness length z_0 corresponding to $R = 2.15 \times 10^{-3}$ is 0.12 cm from Table 2. By using the first approximation of G and taking $z_0 = 0.11$, 0.12, ..., 0.15 cm, five calculated results are obtained. It is found that for $z_0 = 0.14$ cm, the calculated depth-averaged harmonics

$$\bar{U} = 56.9, \quad \bar{\xi} = 1.^{\circ}1, \quad \bar{V} = 20.2, \quad \bar{\eta} = 10.^{\circ}9 \tag{7.3}$$

are the closest to the observed values. Therefore the value of 0.14 cm is considered the best for the station.

Comparison of the calculated values in (7.3) with the observed values in Table 3 shows small deviation, which can be attributed to the inaccuracy of G mainly due to inadequate expression (6.9). This means a small adjustment of G is required. Since there is no simple and definite way to improve expression (6.9) or R, the harmonics in (7.2) are revised by adding the difference of those of (7.2) and (7.3) to the original values. Thus in place of (7.2), $\bar{w}$ is given by

$$\bar{w} = 57.9 \cos(\sigma t - 0.^{\circ}1) + i\, 20.2 \cos(\sigma t - 13.^{\circ}7) \tag{7.4}$$

and is inserted to (6.8) and (6.9) to obtain a further approximation of G. With this G and $z_0 = 0.14$ cm, the numerical calculation gives

$$\bar{U} = 57.4, \quad \bar{\xi} = 0.^{\circ}5, \quad \bar{V} = 20.2, \quad \bar{\eta} = 12.^{\circ}3, \tag{7.5}$$

which is very close to the observed harmonics. This suggests that further adjustment of G may be unnecessary. The calculated harmonics at different depths are also listed in Table 3. The mean deviation of the amplitudes and the phases of calculated harmonics from observed ones is 1.3 cm s^{-1} and 0.°7, respectively. The agreement seems to be satisfactory considering the accuracy of the measurements. For the x-component, which is the major component, the comparison is also shown in Fig. 4. The logarithmic profile calculated from the following formula is also shown in a broken line:

$$U = \frac{[(3/8)\pi F_b]^{1/2}}{k_0} \ln \frac{z + z_0}{z_0}, \tag{7.6}$$

where F_b represents the amplitude of the constituent of τ'_{bx} as $\tau'_{bx} = F_b \sin \sigma t$ and $(3\pi/8) F_b$ is thus the maximum of τ'_{bx} expressed by (6.9) approximately. The value of F_b is 6.381 cm^2 s^{-2} from the numerical solution. The figure suggests that the velocity profile is almost logarithmic around the time of the maximum speed. When the water is sufficiently deep, the velocity may show the logarithmic profile only near the bottom.

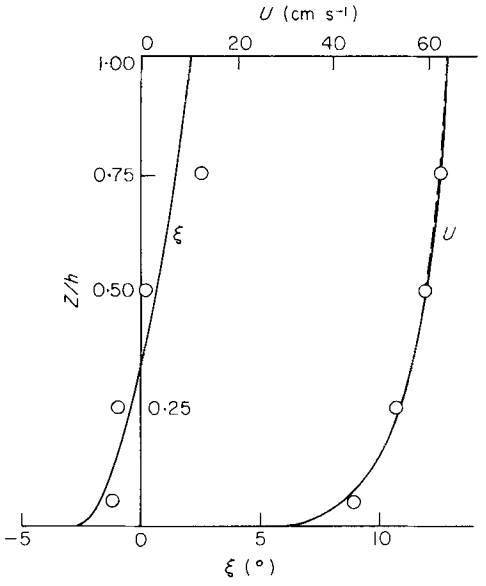

Figure 4. Vertical profiles of the amplitude and phase-lag of u.

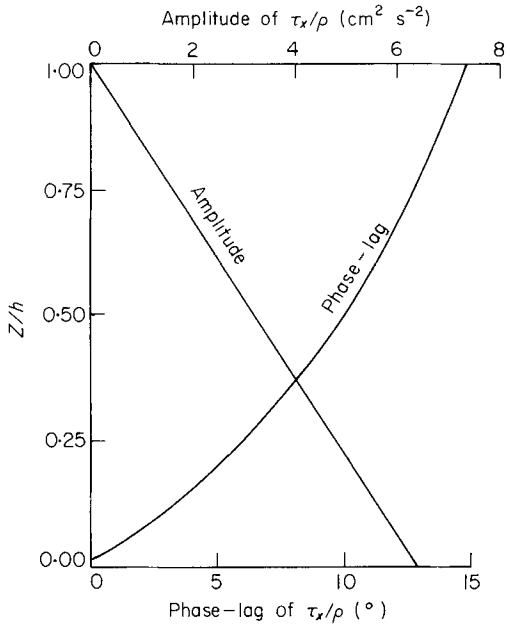

Figure 5. Vertical profiles of the amplitude and phase-lag of τ_x/ρ.

The vertical profile of the shearing stress is shown in Fig. 5. The curve of the amplitude of τ_x' is almost a straight line. The time lag of the maximum stress increases with increasing elevation. Compared with Fig. 4, it can be seen that the phase of the stress always lags that of the velocity with increasing degree at a higher point from the bottom.

The vertical variation of the coefficient of eddy viscosity ν can be given by $\nu = l^2 \mid \partial w/\partial z \mid$

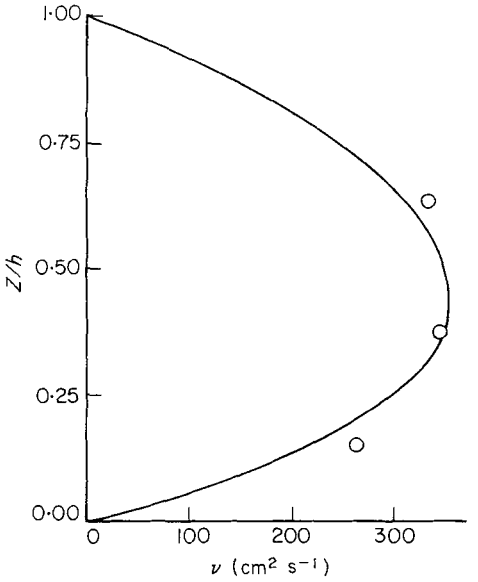

Figure 6. Vertical profile of the coefficient of eddy viscosity ν at time of peak flow. Small circles indicate the observed values by Bowden & Fairbairn (1952).

and hence is dependent on the expression of the mixing length, which is in turn dependent on μ for the upper layer. The calculated vertical distribution of ν corresponding to the peak current is shown in Fig. 6. The maximum value appears a little lower than at the middle depth. BF have given the observed eddy viscosity for their three records, nos 2, 7 and 11. The averaged values of these three records for the depth 0.375 h, 0.625 h and 0.85 h are also marked on Fig. 6 and are seen as close to the calculated curve.

In order to show how the eddy viscosity coefficient varies with time, the depth-averaged coefficient $\bar{\nu}$ is plotted against time in Fig. 7. For comparison the magnitude of the depth-averaged current $|\bar{w}|$ is also plotted. These curves show that the eddy viscosity variation is asymmetrical with time and lags the velocity magnitude variation. The minimum value of eddy viscosity occurs about half an hour after the slack time. If the difference between the phases of the eddy viscosity and the speed is disregarded, the relation

$$\bar{\nu} = 2.7 \times 10^{-3} h \, |\bar{w}| \tag{7.7}$$

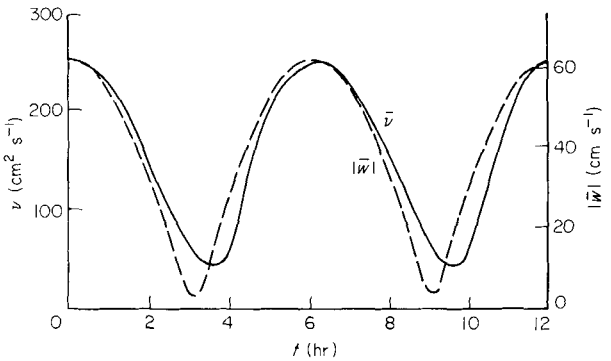

Figure 7. Time-variation of the depth-averaged coefficient of eddy viscosity $\bar{\nu}$ in relation to the magnitude of the depth-averaged velocity $|\bar{w}|$.

is a tolerable approximation. For a steady flow in a non-rotating system the corresponding coefficient is 2.6×10^{-3} for $z_0 = 0.14$ cm, $h = 15.4$ m and $\mu = 1.2$ according to Table 2. The difference is of little significance.

8 Concluding remarks

The effect of bottom friction on tidal currents is a classical hydrodynamic problem, though the dissipation of tidal energy by the friction on the continental shelf of the world ocean is far more important in geophysics. Our understanding of the dissipation mechanism due to the friction and turbulence in shallow waters is far from complete. One approach is to measure directly Reynolds' stresses including the frictional stress. However, this needs special instrumentation which is to be developed and may also require field experiments extensive both in time and space for securing universal validity. The other approach is parameterization of turbulence and friction and then to determine the parameters by fitting the observed current data to the computed values. Tidal current data almost routinely obtained in the shallow waters may be used for determining those parameters which are reasonable such as eddy viscosity, mixing length and friction coefficient. However, this approach may have some pitfalls if the parameterization is quite inadequate.

Profiles of amplitudes and phases of tidal constituents for a constant eddy viscosity may be applied to observed data, for instance, those of CUE (Coastal Upwelling Experiment) in 1972 and 1973 off the Oregon Coast (e.g. Kundu & Allen 1976). We do not do this here for two reasons. First, the vertical spacing of the current meters seems to be too coarse, particularly near the bottom, to resolve the effect of the bottom friction. Secondly, the published data reports do not list harmonic analysis but spectral analysis. The latter may be used for determining the eddy viscosity by comparing variations of the spectral peaks of different tidal frequencies and their shape at different depths with theoretical spectra obtained from a solution of equation (2.4). However, this procedure necessitates some assumed spectrum of G and may not justify the troubles involved. The mixing length hypothesis and quadratic law of the bottom friction seem to be more promising as seen from a good agreement between the observed and numerical results. However, it may need more data of current measurements at closely spaced heights above the bottom to confirm their universal validity. It is suggested that in the future experiments in the shallow waters of the stratified case may be avoided in order to exclude complexities from effects of turbulence by stratification and from internal wave motion and also the bottom may be flat and free from topographic turbulence.

Acknowledgments

This work was partially supported by the Office of Naval Research and NASA Wallops Flight Center.

References

Bowden, K. F., 1962. Turbulence, in *The Sea*, **1**, 802–825, ed. Mill, M. N., Wiley (Interscience), New York.

Bowden, K. F. & Fairbairn, L. A., 1952. A determination of the frictional forces in a tidal current, *Proc. R. Soc. A*, **214**, 371–392.

Bowden, K. F., Fairbairn, L. A. & Hughes, P., 1959. The distribution of shearing stresses in a tidal current, *Geophys. J. R. astr. Soc.*, **2**, 288–305.

Bowden, K. F. & Hamilton, P., 1975. Some experiments with a numerical model of circulation and mixing in a tidal estuary, *Estuar. coast. Mar. Sci.*, **3**, 281–301.

Defant, A., 1961. *Physical Oceanography,* vol. II, 323–337, Pergammon Press, New York.

Godin, G., 1972. *The Analysis of Tides,* pp. 147–148, University of Toronto Press.

Heathershaw, A. D., 1979. The turbulent structure of the bottom boundary layer in a tidal current, *Geophys. J. R. astr. Soc.,* **58,** 395–430.

Ichiye, T., 1955. On the friction in the tidal current, *Oceanogrl Mag.,* **7,** 55–77.

Johns, B., 1966. On the vertical structure of tidal flow in river estuaries, *Geophys. J. R. astr. Soc.,* **12,** 103–110.

Johns, B., 1969a. On the representation of the Reynolds stress in a tidal estuary, *Geophys. J. R. astr. Soc.,* **17,** 39–44.

Johns, B., 1969b. Some consequences of an inertia of turbulence in a tidal estuary, *Geophys. J. R. astr. Soc.,* **18,** 65–72.

Johns, B., 1970. On the determination of the tidal structure and residual current system in a narrow channel, *Geophys. J. R. astr. Soc.,* **20,** 159–175.

Kagan (Cohen), B. A., 1964. On the profile of the longitudinal velocity component of a tidal current in a deep channel, *Oceanology,* **4,** 778–787.

Kagan (Cohen), B. A., 1966. On the structure of the tidal flow in the sea, *Izv. Acad. Sci. USSR Atmos. Ocean. Phys. Ser.,* **2,** 575–581.

Kundu, P. K. & Allen, J. A., 1976. Some three-dimensional characteristics of low-frequency current fluctuations near the Oregon coast. *J. Phys. Oceanogr.,* **6,** 181–199.

Montgomery, R. B., 1943. Generalization for cylinders of Prandtl's linear assumption for mixing length, *Ann. N.Y. Acad. Sci.,* **44,** (1), 81–103.

Proudman, J., 1953. *Dynamical Oceanography,* pp. 310–315, Methuen, London.

Reid, R. O., 1957. Modification of the quadratic bottom-stress law for turbulent channel flow in the presence of surface wind-stress, *Beach Erosion Board Technical Memorandum No. 93,* Corps of Engineers, USA.

Schlichting, H., 1968. *Boundary-Layer Theory,* 6th edn, p. 568, McGraw-Hill, New York.

Sverdrup, H., 1927. Dynamics of tides on the North Siberian Shelf, *Geofys. Publr,* **4,** (5), Oslo.

Thorade, H., 1931. Probleme der Waserwellen, *Probleme kosm. Phys.,* **14,** 152–159.

Wimbush, M. & Munk, W., 1970. The benthic boundary layer, in *The Sea,* **4,** 731–758, ed. Maxwell, A. E., Wiley (Interscience), New York.